Mineralogical Magazine (2024), **88**, 493–502
doi:10.1180/mgm.2024.50

CAMBRIDGE UNIVERSITY PRESS

Article

High-temperature behaviour of fluorcarletonite, $KNa_4Ca_4Si_8O_{18}(CO_3)_4(F,OH)\cdot H_2O$, from the Murun Alkaline Complex, Russia, appraised by experimental and theoretical methods

Ernesto Mesto[1], Maria Lacalamita[1]*, Ekaterina Kaneva[2,3], Roman Shendrik[2], Alexander Bogdanov[2], Marcello Merli[4] and Emanuela Schingaro[1]

[1]Earth and Geoenvironmental Sciences Department, University of Bari Aldo Moro, via E. Orabona 4, I-70125 Bari, Italy; [2]Vinogradov Institute of Geochemistry, Siberian Branch of the Russian Academy of Sciences, 1a Favorsky Str., 664033 Irkutsk, Russia; [3]Sidorov Mineralogical Museum, Irkutsk National Research Technical University, 83 Lermontov Str., 664074 Irkutsk, Russia; and [4]Earth and Sea Sciences Department, University of Palermo, via V. Archirafi 36, I-90123 Palermo, Italy

Abstract

The thermal behaviour of fluorcarletonite, $KNa_4Ca_4Si_8O_{18}(CO_3)_4(F,OH)\cdot H_2O$, from the charoitites of the Severny district at the Malyy Murun massif, Murun complex, NW Aldan Shield, Siberia, Russia, has been investigated in order to understand the temperature-induced changes in the crystal structure of this rare silicate. The study has been carried out combining *in situ* high-temperature single-crystal X-ray diffraction (*T* range 25–550°C), *ex situ* high-temperature Fourier-transform infrared spectroscopy (25–700°C) and *ab initio* calculations. An increasing trend of lattice parameters and cell volume was observed in the 150–550°C temperature range, when the mineral underwent a progressive dehydration process. At 550°C ~40% water loss was detected. If compared with the fluorcarletonite structure at room temperature, the partially dehydrated fluorcarletonite shows: the same space group (*P*4/*mbm*); increased distances between the oxygens of the H_2O molecules (O11w and O12w) and their Na-centred octahedral cations (Na1 and Na2, respectively); distortion of the four- and six-member tetrahedral rings of the double silicate layer. The dehydration process mainly involves the oxygen at the O11w site which has a different local environment with respect to the oxygen at the O12w site. At $T > 600$°C, the complete dehydration is accompanied by deprotonation of the OH groups substituting for the F atoms and by the collapse of the structure when the CO_2 is released. The adopted approach allowed definition of the temperature thresholds at which modifications occur in the fluorcarletonite crystal structure when subjected to controlled heating conditions. Our findings contribute to assessment of stability, reactivity and, more generally, the thermal behaviour of sheet silicates with fluorcarletonite-like topology.

Keywords: fluorcarletonite; high temperature; single-crystal X-ray diffraction; infrared spectroscopy; *ab initio* calculations

(Received 18 March 2024; accepted 4 June 2024)

Introduction

Fluorcarletonite, $KNa_4Ca_4Si_8O_{18}(CO_3)_4(F,OH)\cdot H_2O$, from the Malyy Murun syenite massif, Aldan Shield, Siberia, Russia, was approved recently as a new mineral species by the Commission on New Minerals, Nomenclature and Classification of the International Mineralogical Association (IMA2019-038, Kaneva *et al.*, 2019). The first description of this mineral was provided by Kaneva *et al.* (2020a), who also explained the difference with respect to the structural analogue carletonite, $KNa_4Ca_4Si_8O_{18}(CO_3)_4(OH,F)\cdot H_2O$ (Kaneva *et al.*, 2023). The latter is a rare mineral named after Carleton University in Ottawa, and found in the Poudrette quarry, Mont Saint-Hilaire, Canada (Chao, 1971, 1972). Fluorcarletonite and carletonite undergo replacement of F ions with OH groups (or vice versa) which causes no significant structural differences as the fluorine and OH radii are very close (1.30 and 1.36 Å, Shannon, 1976) and the hydrogen does not significantly affect the local environment. The reported fluorine content in the crystal chemical formula of fluorcarletonite varies in the range of 0.53–0.98 atoms per formula unit (apfu) (Kaneva *et al.*, 2020a, 2023) whereas for carletonite from Mont Saint-Hilaire massif F = 0.41 apfu (Chao, 1971) or $0.36 \leq F \leq 0.41$ apfu (Kaneva *et al.*, 2023) has been reported.

In the peripheral regions of zoned grains of Russian fluorcarletonite, the carletonite composition has been detected (Kaneva *et al.*, 2020a, 2022) which implies that, conversely, fluorcarletonite might occur in the rocks of Mount Saint-Hilaire Massif, Canada. However, pure hydroxyl or fluorine end-members have not yet been found. The occurrence of carletonite in lateritic soils covering carbonatites, ijolites, nepheline syenites and fenites of the Bingo carbonate complex, Democratic Republic of Congo (Kasay, 2018; Kasay *et al.*, 2021) should also be confirmed by more accurate chemical and X-ray diffraction investigations.

Fluorcarletonite and carletonite are described as double-layer sheet silicates based on the $[4.8^2]_{16}$ net with an arrangement of upward-pointing tetrahedra (u) and downward-pointing tetrahedra (d) showing $(u^2d^2)_4(ududud)_4$ configuration and 1:2.25

***Corresponding author:** Maria Lacalamita; Email: maria.lacalamita@uniba.it
Associate Editor: G. Diego Gatta
Cite this article: Mesto E., Lacalamita M., Kaneva E., Shendrik R., Bogdanov A., Merli M. and Schingaro E. (2024) High-temperature behaviour of fluorcarletonite, $KNa_4Ca_4Si_8O_{18}(CO_3)_4(F,OH)\cdot H_2O$, from the Murun Alkaline Complex, Russia, appraised by experimental and theoretical methods. *Mineralogical Magazine* **88**, 493–502. https://doi.org/10.1180/mgm.2024.50

T:O ratio (Hawthorne *et al.*, 2019). In detail, $[Si_8O_{18}]^{4-}$ sheets, extending in the *a*–*b* plane, consist of four-member rings with two upward- and two downward-pointing tetrahedra, and eight-member rings with alternately upward- and downward-pointing tetrahedra. Two adjacent single layers are interconnected by sharing a common oxygen of downward-pointing tetrahedra. The $[Si_8O_{18}]^{4-}$ sheets are connected with sheets consisting of $NaO_4^{2-}F^-(H_2O)$ and $NaO_5^{2-}(H_2O)$ octahedra, NaO_8^{2-}, $CaO_7^{2-}F^-$ or CaO_8^{2-} and KO_{10}^{2-} polyhedra. The structural role of H_2O molecules is different, as one molecule is bonded to an interstitial cation and acts as a bond-valence transformer, the other one is non-transformer (Hawthorne, 1992). Two independent CO_3-groups are linked to Na- and Ca-polyhedra.

The crystal structure of fluorcarletonite was determined experimentally at low temperature (100 K; Kaneva *et al.*, 2020a) and room temperature (RT, Kaneva *et al.*, 2023) but was also simulated in order to define the position of the hydrogens and the most energetically favourable orientations of the H_2O (Kaneva *et al.*, 2023). The geometrical parameters of fluorcarletonite were found very similar to those of carletonite although they are distinct mineral species with individual peculiarities. In particular, the carletonite structure exhibits a splitting of the K atom over two sites, with 89% and 6% approximate occupancy, whereas the K position in fluorcarletonite is ordered (Kaneva *et al.*, 2023).

In Kaneva *et al.* (2022, 2023) the luminescence and the gemmological properties of fluorcarletonite were also completely characterised. The multi-coloured appearance of the fluorcarletonite-containing rocks, which is due to the association of various minerals, makes these samples very attractive gem materials for incorporation into jewellery and ornamental items (Kaneva *et al.*, 2020a, 2022).

The thermal behaviour of fluorcarletonite has not yet been assessed thoroughly. Chao (1971) studied the decomposition of carletonite by means of *ex situ* high-temperature X-ray powder diffraction (HT XRPD) analyses and differential thermal analysis. The structure breakdown was associated to the release of CO_2 (but also of H_2O) evidenced by a strong endothermic peak in the DTA curve at 692°C. Kaneva *et al.* (2020a) used thermogravimetric (TG) and differential scanning calorimetric (DSC) analyses on fluorcarletonite and found that the mineral underwent dehydration from 45 to 315°C, loss of CO_2 from 630 to 1134°C and defluorination from 1136 to 1500°C.

In the present study, the thermal behaviour of fluorcarletonite was appraised via a combination of experimental (*in situ* high-temperature single-crystal X-ray diffraction, HT SCXRD; *ex situ* high-temperature Fourier transform infrared spectroscopy, HT FTIR) and theoretical (*ab initio* simulations) methods, thus filling the gaps from previous studies and providing new insights into the structural variations of minerals with complex bond topology in relations to temperature changes.

Geological context and sample description

The fluorcarletonite studied occurs in charoitites of the Severny district at the Malyy Murun massif, Murun complex, NW Aldan Shield, Siberia, Russia. The ultra-agpaitic alkaline Murun complex was dated 137–128 Ma and had a complex geological history characterised by four igneous stages (early intrusive, main intrusive, volcanic and late intrusive) and by hydrothermal activity represented by quartz veins with rutile–brookite–anatase mineralisation (see more details in Vladykin, 2009; Borovikov *et al.*, 2018; Ivanov *et al.*, 2018; Vladykin *et al.*, 2018).

Kaneva *et al.* (2020a, 2022) carried out the mineralogical and petrographic examination of a polished slab of a fluorcarletonite-containing rock sample from the Malyy Murun massif and found that the mineral paragenesis is defined by the crystallisation of alkali silicates (fluorcarletonite, charoite, apophyllite-(KF), aegirine and pectolite), quartz, apatite and microcline, by the formation of copper and lead sulfides as well as native copper, and by the alteration of primary rock-forming minerals with formation of secondary apophyllite-(KF) and wollastonite caused by supergene conditions. Fluorcarletonite appears as allotriomorphic grains, blue in colour, and forming close intergrowths with fluorapophyllite-(K) and pectolite.

In the present study, fluorcarletonite from the same rock sample as in Kaneva *et al.* (2020a, 2022, 2023) was considered. The authors reported for fluorcarletonite the following average crystal chemical formula: $K_{0.99}Na_{3.86}Ca_{3.87}Sr_{0.02}Si_{7.99}Al_{0.01}O_{18}(CO_3)_{3.81}(F_{0.60}OH_{0.40})\cdot 1.42H_2O$.

Methods

In situ HT SCXRD

Single crystals of fluorcarletonite suitable for the X-ray diffraction investigation were selected under an optical microscope, glued on the tip of a glass fibre and mounted on a goniometer head. The *in situ* high-temperature X-ray diffraction experiment was carried out with a Bruker AXS APEX II diffractometer equipped with Mo*K*α radiation (λ = 0.71073 Å), a CCD area detector and a home-made heating device (Zema *et al.*, 2022). A crystal (labelled Fcarl_1, 0.50 × 0.21 × 0.20 mm^3) with good diffraction behaviour was heated in air from 25 to 450°C in steps of 25°C, with a heating rate of 1°C/min. After each heating step, the crystal was equilibrated for ca. 30 min before the acquisition of a new data collection. A total of 18 data collections was acquired: those at 25 and in the *T* range 125–450°C lasted ca. 6 hours ($2\theta_{max}$ = 66° and d_{hkl} = 0.65 Å) whereas those from 50 to 100°C lasted 1 hour ($2\theta_{max}$ = 60° and d_{hkl} = 0.7 Å). The experiment was repeated by heating a second crystal (labelled Fcarl_2, 0.63 × 0.35 × 0.30 mm^3) from 25 to 550°C with the same operating conditions. However, in this case all the data collections lasted ca. 1 hour ($2\theta_{max}$ = 72° and d_{hkl} = 0.60 Å). Attempts were also made to heat the Fcarl_2 crystal up to 625°C but loss of crystallinity was observed.

The diffractometer operated at 50 kV and 30 mA. The collection strategies were optimised with the *Apex* program suite (Bruker 2010); data reductions were done using the software *SAINT* (Bruker, 2007); empirical absorption corrections were applied using *SADABS* (Bruker, 2009); and structure refinements were performed with the program *CRYSTALS* (Betteridge *et al.*, 2003) in the space group *P*4/*mbm* using reflections with $I > 3\sigma(I)$ and starting from the atomic coordinates of fluorcarletonite reported in Kaneva *et al.* (2023). The refined parameters were: scale factor, atomic positions and anisotropic displacement parameters. The occupancies of the cation sites were constrained to 1 whereas the H_2O occupancies (O11w, O12w oxygen atoms) were refined for all the data collections. The analysis of the difference-Fourier maps showed the presence of residual electron density peaks <0.8 $e^-/Å^3$.

Details on data collection and structure refinements at 25, 100, 200, 300 and 450°C for the Fcarl_1 crystal, and at 25 and 550°C for the Fcarl_2 crystal are reported in Table 1. Selected bond distances at 25, 450 and 550°C are provided in Table 2. Selected anion distances and angles are listed in Table 3. Crystallography Information Files of all the crystal structures refined for Fcarl_1

https://doi.org/10.1180/mgm.2024.50 Published online by Cambridge University Press

Table 1. Crystallographic data and experimental conditions for fluorcarletonite at 25, 100, 200, 300 and 450°C for the Fcarl_1 crystal, and at 25 and 550°C for the Fcarl_2 crystal.

	Fcarl_1					Fcarl_2	
	25°C	100°C	200°C	300°C	450°C	25°C	550°C
Crystal data							
Space group	*P*4/*mbm*	*P*4/*mbm*	*P*4/*mbm*	*P*4/*mbm*	*P*4/*mbm*	*P*4/*mbm*	*P*4/*mbm*
a (Å)	13.2077(4)	13.1962(13)	13.2293(4)	13.2397(3)	13.2584(3)	13.2082(3)	13.2782(4)
c (Å)	16.7234(5)	16.7190(16)	16.7489(6)	16.7609(5)	16.7822(4)	16.7219(4)	16.8151(4)
V (Å^3)	2917.3(2)	2911.4(6)	2931.3(2)	2938.01(16)	2950.06(15)	2917.25(15)	2964.68(19)
Data collection							
Measured reflections	18888	18945	49275	55109	55439	18476	18723
Independent reflections	2444	2457	3826	3847	3860	2340	2386
$R_{merging}$ [$R_{(int)}$] (%)	8.1	8.4	6.3	6.5	6.7	6.6	7.1
h_{min}, h_{max}	−18, 17	−19, 17	−21, 22	−22, 22	−22, 22	−18, 18	−18, 18
k_{min}, k_{max}	−18, 12	−18, 11	−21, 15	−22, 15	−22, 15	−18, 10	−10, 18
l_{min}, l_{max}	−23, 23	−23, 22	−27, 27	−27, 27	−27, 27	−22, 23	−22, 22
Refinement							
Reflections used ($I > 3\sigma(I)$)	1736	1700	2573	2520	2387	1742	1632
No. of refined parameters	144	144	144	144	144	144	144
Gof [a]	1.121	1.111	1.049	1.018	0.999	1.022	1.018
R_1 [b] [on *F*] (%)	3.34	3.43	3.07	3.04	3.15	2.83	3.04
wR_2 [c] [on F^2] (%)	4.30	4.29	3.17	3.52	3.81	3.14	3.52
$\Delta\rho_{min}/\Delta\rho_{max}$ (e^-/Å^3)	−0.62, 0.79	−0.64, 0.59	−0.51, 0.67	−0.76, 0.77	−0.57, 0.55	−0.57, 0.65	−0.76, 0.77

Notes: [a]Goodness of fit = $[\Sigma[w(F_o^2-F_c^2)^2]/(N-p)]^{1/2}$, where *N* and *p* are the number of reflections and parameters, respectively. [b]$R_1 = \Sigma[|F_o| - |F_c|]/\Sigma|F_o|$. [c]$wR_2 = [\Sigma[w(F_o^2-F_c^2)^2]/\Sigma[w(F_o^2)^2]]^{1/2}$, $w = 1.0/[A[0]*T[0]'(X)+A[1]*T[1]'(X) \ldots +A[NP-1]*T[NP-1]'(X)]$ (Chebyshev optimised weights). The optimised parameters for each refinement are reported in the deposited Crystallography Information Files.

and those at 25 and 550°C for Fcarl_2 are submitted as supplementary material together with atomic coordinates, site occupancy and displacement parameters at selected temperature (Table S1) and bond-valence data at 25 and 550°C (Table S2). Bond valence calculations were performed using the parameters from Brown and Altermatt (1985), and Breese and O'Keeffe (1991) for the cation–fluorine bonds.

Ex situ HT FTIR

Fourier-transform infrared spectra were measured using an FT−801 spectrophotometer (Simex, Russia). Pelletised powdered samples were analysed at a resolution of 2 cm^{-1} by collecting a total of 32 scans for each spectrum in the *T* range 25–700°C. The *ex situ* experiment was performed by using the procedure described in previous publications (Kaneva *et al.*, 2020b; Kaneva and Shendrik, 2022) and briefly summarised as follows: (1) a mixture of fluorcarletonite and preliminarily dried pure KBr powder was pressed into a transparent tablet and heated to a target temperature for 5 min; (2) the same heating temperature and heating time were applied for pure dried KBr pellets, used as reference; (3) both the mixture and pure KBr pellets were cooled down to room temperature and the IR absorption spectra were measured again. These steps were repeated during the heating from 100°C up to 700°C.

Table 2. Selected bond distances (Å) derived from the structure refinement of the fluorcarletonite crystals studied at 25 and 450°C (Fcarl_1) and at 550°C (Fcarl_2).

	Fcarl_1		Fcarl_2		Fcarl_1		Fcarl_2
	25°C	450°C	550°C		25°C	450°C	550°C
*Si*1–O1	1.593(2)	1.5887(16)	1.586(3)	*Na*1–O3 (×4)	2.347(2)	2.3854(15)	2.408(3)
*Si*1–O2	1.5954(19)	1.5958(14)	1.589(2)	*Na*1–F13	2.620(4)	2.623(4)	2.637(6)
*Si*1–O5	1.6206(12)	1.6179(9)	1.6149(15)	*Na*1–O11w	2.349(7)	2.437(11)	2.59(3)
*Si*1–O6	1.6122(11)	1.6078(8)	1.6059(12)	<*Na*1–O,F>	2.393(2)	2.434(3)	2.477(2)
<*Si*1–O>	1.605(1)	1.603(4)	1.599(1)				
				*Na*2–O4	2.464(3)	2.498(3)	2.520(5)
*Si*2–O1	1.626(2)	1.6197(15)	1.622(3)	*Na*2–O7 (×2)	2.392(2)	2.4046(19)	2.416(3)
*Si*2–O2	1.6291(19)	1.6250(14)	1.626(2)	*Na*2–O10 (×2)	2.345(2)	2.371(2)	2.384(4)
*Si*2–O3	1.5764(19)	1.5765(13)	1.573(2)	*Na*2–O12w	2.886(3)	3.065(16)	3.16(2)
*Si*2–O4	1.6286(11)	1.6289(8)	1.6276(13)	<*Na*2–O>	2.471(2)	2.519(1)	2.547(4)
<*Si*2–O>	1.615(1)	1.613(2)	1.612(1)				
				*Na*3–O7 (×4)	2.548(2)	2.568(2)	2.581(3)
*Ca*1–O3	2.3757(19)	2.3875(14)	2.396(2)	*Na*3–O8 (×2)	2.396(3)	2.418(3)	2.419(4)
*Ca*1–O3'	2.4388(18)	2.4526(14)	2.461(2)	*Na*3–O9 (×2)	2.544(3)	2.569(3)	2.583(5)
*Ca*1–O7	2.526(2)	2.5493(16)	2.565(3)	<*Na*3–O>	2.509(1)	2.531(1)	2.541(2)
*Ca*1–O7'	2.548(2)	2.5662(16)	2.577(3)				
*Ca*1–O8	2.4504(5)	2.4579(4)	2.4628(7)	*K*1–O2 (×4)	3.205(2)	3.2269(16)	3.240(3)
*Ca*1–O9	2.4333(9)	2.4531(8)	2.4683(13)	*K*1–O5 (×2)	2.943(3)	2.939(2)	2.938(4)
*Ca*1–O10	2.410(2)	2.4176(18)	2.416(3)	*K*1–O10 (×4)	2.800(2)	2.816(2)	2.820(3)
*Ca*1–F13	2.5054(7)	2.5129(5)	2.5152(9)	<*K*1–O>	2.991(1)	3.005(1)	3.012(1)
<*Ca*1–O,F>	2.461(2)	2.474(1)	2.483(2)				
*C*1–O7 (×2)	1.282(3)	1.2864(19)	1.282(3)	*C*2–O10 (×2)	1.276(3)	1.272(2)	1.267(3)
*C*1–O9	1.293(5)	1.278(3)	1.265(6)	*C*2–O8	1.301(4)	1.299(4)	1.304(6)

https://doi.org/10.1180/mgm.2024.50 Published online by Cambridge University Press

Table 3. Selected anion bond distances (Å) and angles (°) derived from the structure refinement of the fluorcarletonite crystals studied at 25, 100, 200, 300 and 450°C (Fcarl_1), and at 550°C (Fcarl_2).

	25°C	100°C	200°C	300°C	450°C	550°C
O11w–O11w'	2.823(13)	2.806(15)	2.790(12)	2.756(14)	2.60(2)	2.26(6)
O12w–O12w'	1.95(4)	1.85(5)	1.76(4)	1.67(4)	1.49(5)	1.28(7)
O6–O6	4.005(6)	3.986(6)	3.987(4)	3.965(4)	3.924(5)	3.867(8)
O5–O5	3.221(5)	3.228(6)	3.261(4)	3.288(4)	3.342(5)	3.424(8)
O1–O2	2.581(3)	2.578(3)	2.5822(19)	2.5816(19)	2.578(2)	2.581(4)
Angles						
O5–O6–O5	75.19(6)	75.53 (7)	76.11(4)	76.97(5)	77.99(5)	81.03(9)
O2–O1–O3	100.43(9)	100.67(9)	100.82(6)	101.10(6)	101.31(7)	102.0(1)

Ab initio calculation

Ab initio modelling of IR spectra was carried out using the "VASP" *ab initio* code (Kresse and Hafner, 1993), employing a pseudopotential method and plane wave basis sets. Exchange and correlation were expressed in terms of the PBEsol function (Perdew *et al.*, 2008), with an energy cutoff for plane wave basis sets of 400 eV. The Brillouin zone sampling was performed using the gamma point only.

The geometry was relaxed until the maximal force acting on an atom was <0.001 eV/Å, followed by phonon calculation using the 'Phonopy' code (harmonic approximation), Togo and Tanaka (2015). The infrared spectra were simulated with the 'Phonopy–Spectroscopy' tool, with a single model containing fully populated O11w and O12w (six H_2O molecules) being calculated. The methodology of assigning the calculated modes has been described in detail in Bogdanov *et al.* (2021).

The presence of hydrogens in the structure can involve a significant anharmonicity, therefore the above simulations have been coupled to *ab initio* molecular dynamics runs, carried out by means of the 'Abinit' code (Gonze *et al.*, 2016), with PBEsol for exchange and correlation functions, and energy cut off converged to 90 eV. NVT ensemble molecular dynamics calculations have been carried out at 27, 327 and 627°C. For all the runs, the same (idealised) starting *P*1 geometry obtained from *ab initio* modelling in Kaneva *et al.* (2023) has been adopted (with a = 13.2256 Å, c = 16.7329 Å, V = 2926.9 Å^3 and 226 atoms). Given the large unit cell and the consequent great number of atoms, no supercell has been adopted in the molecular dynamics simulations. The systems were equilibrated after 10^3 steps, with a time step of 2.5 fs.

Results

Crystal structure description at room and high temperature

Room-temperature refinement in space group *P*4/*mbm* converged to R_1 = 3.34% (for Fcarl_1) and 2.83% (for Fcarl_2), wR_2 = 4.30% (for Fcarl_1) and 3.14% (for Fcarl_2), see Table 1. The values of the refined lattice parameters and cell volume were very close for the two crystals studied (a = 13.2077(4) Å, c = 16.7234(5) Å, V = 2917.3(2) Å^3 for Fcarl_1 and a = 13.2082(3) Å, c = 16.7219(4) Å, V = 2917.25(15) Å^3 for Fcarl_2, Table 1) and similar to those in Kaneva *et al.* (2023).

A representation of the complete crystal structure of fluorcarletonite, plotted down the *b* axis, is given in Fig 1. It consists of two tetrahedral sites (*Si*1 and *Si*2), two octahedral independent sites (*Na*1 and *Na*2), two 8-coordinated sites (*Na*3 and *Ca*1), one 10-coordinated site (*K*1), two 3-coordinated sites (*C*1 and *C*2), ten oxygen sites, one F site and two sites occupied by oxygens of H_2O (O11w and O12w sites), Fig. 1 and Table S1. Figure 2, instead, displays a fragment of the fluorcarletonite crystal structure with details on the local environment of the oxygen at the O11w and O12w sites.

The refined occupancies for the oxygens at the O11w and O12w sites at RT were, respectively, 0.93(2) and 0.62(3) for Fcarl_1, and 1.016(17) and 0.650(19) for Fcarl_2 (Table S1). Similar values were found in previous investigations for fluorcarletonite (O11w = 0.833(9) and O12w = 0.535(9) in Kaneva *et al.*, 2020a; O11w = 0.87(1) and O12w = 0.55(2) in Kaneva *et al.*, 2023) as well as for carletonite (Chao, 1972; Kaneva *et al.*, 2023). The $U_{iso/equivalent}$ values of oxygens at the O11w and O12w sites are larger than those of all other atoms (Table S1), consistently with their low bond valence sums (BVS) (Table S2). The thermal motion for these oxygens is particularly pronounced already at room temperature. A similar behaviour was also observed in the case of other hydrated sheet silicates with complex bond topology (Lacalamita *et al.*, 2023).

In addition, the short O12w–O12w distance (1.95(4) Å, Table 3) confirms the occurrence of mutually exclusive positions of nearest oxygens at the O12w site (Kaneva *et al.*, 2023). The values of individual and average bond length distances for tetrahedra, and Na- and Ca-polyhedra of the crystals studied (Table 2) were also very similar to those reported in the literature.

Given the close similarities in the geometrical features of the two crystals, in the text below and in the figures, we will consider the data collected at 550°C for Fcarl_2 in addition to those from 25 to 450°C for Fcarl_1.

With increasing temperature, fluorcarletonite shows no change in symmetry (Table 1). However, the evolution of the normalised unit cell parameters and volume as a function of the temperature (Figs 3 and S1) provides evidence that the unit cell dimensions remain almost constant until ~150–200°C when they start to increase.

The mean atomic number of the oxygen at O12w and especially at the O11w site progressively decreases as the temperature increases (Fig. 4). Considering that the correlation coefficient between occupancies and Uij's of O11w and O12w are < 0.6 both for RT and 550°C measurements, these results point to an overall dehydration of fluorcarletonite at 550°C of ~40%.

The oxygen at the O11w site coordinates the Na1 octahedron together with four O3 atoms of the silicate layer and one F. It points towards an equivalent O11w oxygen, both lying on the *c* axis (Fig. 2). During heating, the *Na*1–O11w bond weakens (0.229 vu and 0.119 vu at 25 and 550°C, respectively, Table S2). In detail, the oxygen moves away from the *Na*1 neighbouring cation (as indicated by the lengthening of the *Na*1–O11w distance

https://doi.org/10.1180/mgm.2024.50 Published online by Cambridge University Press

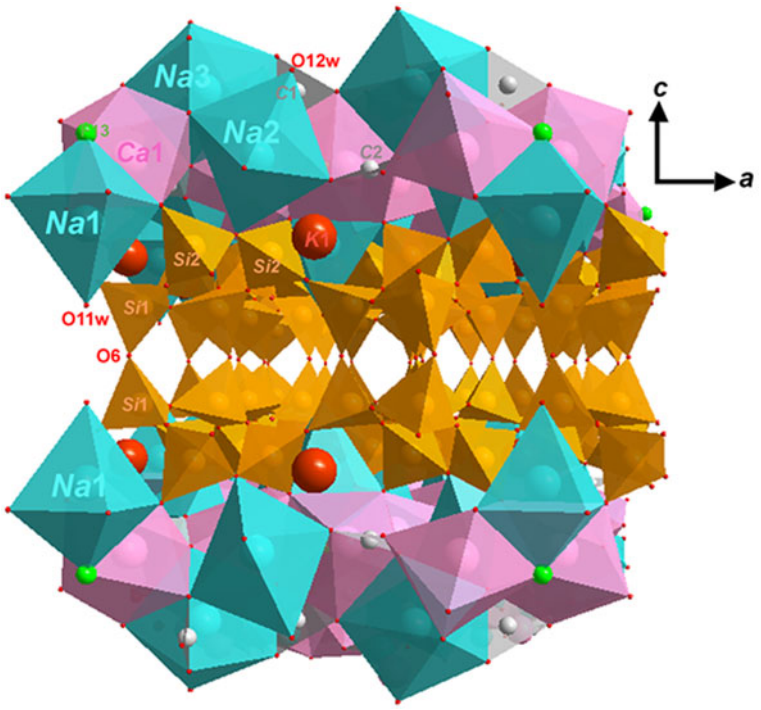

Figure 1. Crystal structure of fluorcarletonite from Murun Massif as seen along *b*. Si-tetrahedra (orange), Na-polyhedra (blue), Ca-polyhedron (pink), K^+ (brown) and C (grey) atoms are represented. Oxygen and fluorine atoms are illustrated in red and green, respectively. Crystal drawings made using *Diamond* software. (*Diamond* – Crystal and Molecular Structure Visualization, Crystal Impact – Dr. H. Putz & Dr. K. Brandenburg GbR, Kreuzherrenstr. 102, 53227 Bonn, Germany, https://www.crystalimpact.de/diamond).

from 2.349(7) to 2.59(3) Å, Table 2) and approaches the equivalent O11w oxygen (as testified by the shortening of the O11w–O11w' distance from 2.822(13) to 2.26(6) Å, Table 3).

The O12w is shared by two *Na*2 octahedra which are also bonded to one O4 atom of the silicate layer, two O7 and two O10 atoms (Fig. 2). The oxygen at O12w receives 0.054 vu at

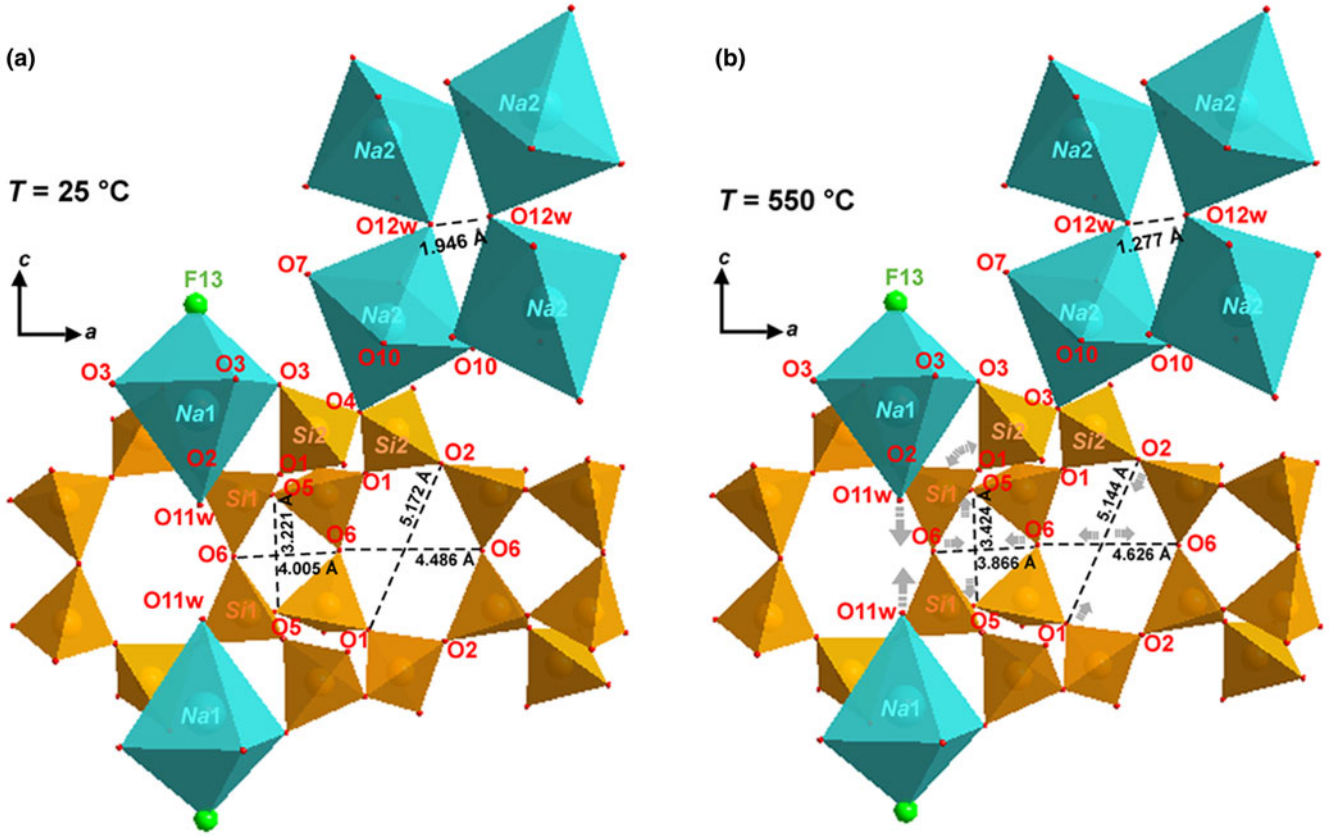

Figure 2. Detail of the crystal structure of fluorcarletonite showing the dimensions of the tetrahedral rings in the *a*-*c* plane at (a) *T* = 25°C and (b) *T* = 550°C. Colours as in Fig. 1.

https://doi.org/10.1180/mgm.2024.50 Published online by Cambridge University Press

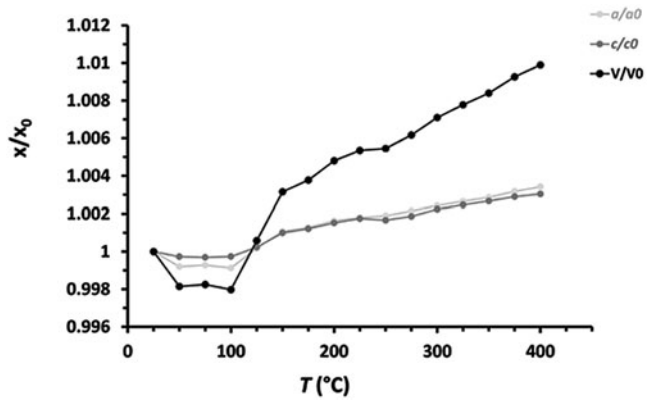

Figure 3. Normalised unit cell parameters and volume of the Fcarl_1 crystal *versus* temperature. Symbols: a/a_0 and b/b_0 (light grey); c/c_0 (dark grey); V/V_0 (black). a_0, b_0, c_0, and V_0 are lattice parameters and unit cell volume at RT, respectively. The size of the symbols is larger than the associated esds.

RT and 0.026 vu at 550°C (Table S2). The water content at the O12w site decreases slightly (from 4.96 to 3.84 m.a.n.'s, e^- at RT and 550°C, respectively, Fig. 4) while the distance of the oxygen at O12w site from the *Na*2 neighbouring cation increases strongly (from 2.886(3) Å at RT to 3.16(2) Å at 550°C, respectively, Table 2). At the same time, the O12w–O12w' distance decreases (from 1.95(4) Å at RT to 1.28(7) Å at 550°C, respectively, Table 3, Fig. 2).

No significant modifications of the geometrical parameters of the *Na*3-, *Ca*1-, and *K*1-polyhedra as well as of the CO_3 groups at 550°C with respect to RT are observed (Table 2).

As concerns the tetrahedral framework, Fig. 2 shows that the linkage between two single tetrahedral layers via the oxygen at the O6 site defines, in the *a*–*c* plane, four- and six-membered tetrahedral rings alternated along *a* and with a mean area $4.0047(37) \times 3.2213(38)$ Å^2 and $5.1720(28) \times 4.4858(37)$ Å^2, respectively, at RT (Fig. 2a). As the temperature increases, a distortion of these rings is observed. In particular, the stretching of the *Si*1 tetrahedra along the *c* direction causes an increment of the O5–O6–O5 angle (from 75.188(63) to 81.029(86)° at RT and 550°C, respectively, Table 3) and, consequently, an elongation of the four-membered tetrahedral rings along the *c* direction

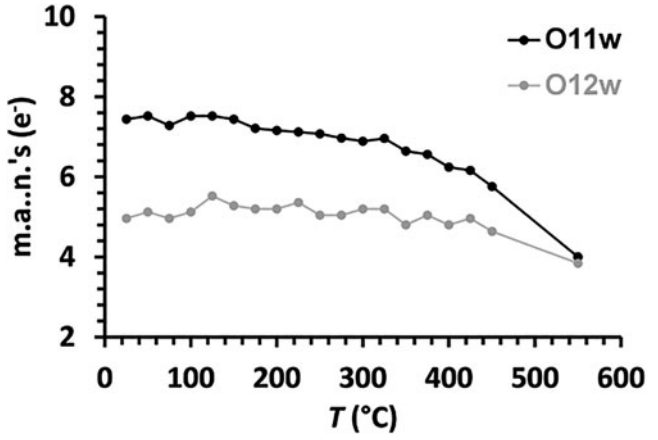

Figure 4. Mean atomic numbers (m.a.n., e^-) for the oxygens at the O11w (black line and symbol) and O12w sites (light grey line and symbol) in fluorcarletonite *versus* temperature.

together with its compression along the *a* direction. On the contrary, the adjacent six-membered tetrahedral ring expands in the *a* direction (compare Fig. 2a and b). A tilting of the *Si*2 tetrahedra has also been observed as revealed by the O2–O1–O3 angle increment from 100.429(87) at 25°C to 102.028(116) at 550°C (Table 3).

High-temperature infrared data

The infrared spectra of fluorcarletonite heated from RT to 700°C are presented in Figs 5 and 6 for the Si–O framework and the O–H stretching vibration regions, respectively.

At low frequencies, weak bands between 500 and 900 cm^{-1} are observed in the spectrum collected at RT (Fig. 5). By increasing the temperature, the bands at 526, 591 and 661 cm^{-1} shift and at $T = 700$°C are found centred at 519, 586 and 655 cm^{-1}, respectively (Fig. S2). The intensity of the bands at 591 and 693 cm^{-1} decreases; the latter trend is also observed for the absorption band in the 802–815 cm^{-1} range which at $T > 400$°C shows a maximum at 808 cm^{-1}. No changes affect the bands at 701, 729, 785 and 875 cm^{-1}.

At higher frequencies, a strong band occurs at 1050 cm^{-1} as also reported elsewhere (Kaneva *et al.*, 2020a) but it is not shown in Fig. 5. The band at 1196 cm^{-1} splits into two bands at 1170 and 1220 cm^{-1} starting from $T = 500$°C. Bands peaking at 1397, 1418, 1451, 1480 and 1525 cm^{-1} with shoulders at 1371 and 1550 cm^{-1}, change their shape during heating (Fig. 5). In particular, the bands at 1418 and 1480 cm^{-1} become less resolved at $T = 600$°C, and the intensities of the 1397 and 1451 cm^{-1} bands decrease slightly.

In the O–H stretching region three main peaks at 3557, 3582 and 3645 cm^{-1} (with a shoulder at 3595 cm^{-1}) are observed at RT (Fig. 6). In the spectra of the annealed fluorcarletonite, the intensity of the peaks at 3557 and 3645 cm^{-1} progressively decreases until they vanish at $T > 200$ and 500°C, respectively. This evolution makes a peak centred at 3690 cm^{-1} more evident starting from $T = 200$°C. At the same temperature, a band centred at 3595 cm^{-1} becomes evident. This band together with that at 3582 cm^{-1} show only minimal changes during heating. Overall, the OH stretching bands are hardly evident at $T = 600$°C. The temperature dependences of these band intensities are given in Fig. S3.

In Fig. 6 very low intensity bands at 2950, 3015 and 3420 cm^{-1} are also shown. The wide absorption at 3420 cm^{-1} disappears after $T = 100$°C while the intensity and position of the bands at 2950 and 3015 cm^{-1} remains unchanged across the whole explored temperature range.

Discussion

Structural evolution under high temperature

The *in situ* high-temperature X-ray diffraction experiment from 25 to 550°C on fluorcarletonite from the Murun massif, Russia provides evidence that the mineral undergoes a thermal expansion of the unit cell volume accompanied by a progressive dehydration. In layered minerals the removal of interlayer H_2O molecules and the reorganisation of the interlayer space usually results in a decrease in the *d*-spacing and, as a consequence, in the shrinking of the unit cell parameters and volume contraction (Bray *et al.*, 1998; Zema *et al.*, 2010; Post *et al.*, 2015). However, in some hydrated sheet silicates with complex bond topology, the tetrahedral framework defines interlayer cavities hosting zeolitic H_2O

https://doi.org/10.1180/mgm.2024.50 Published online by Cambridge University Press

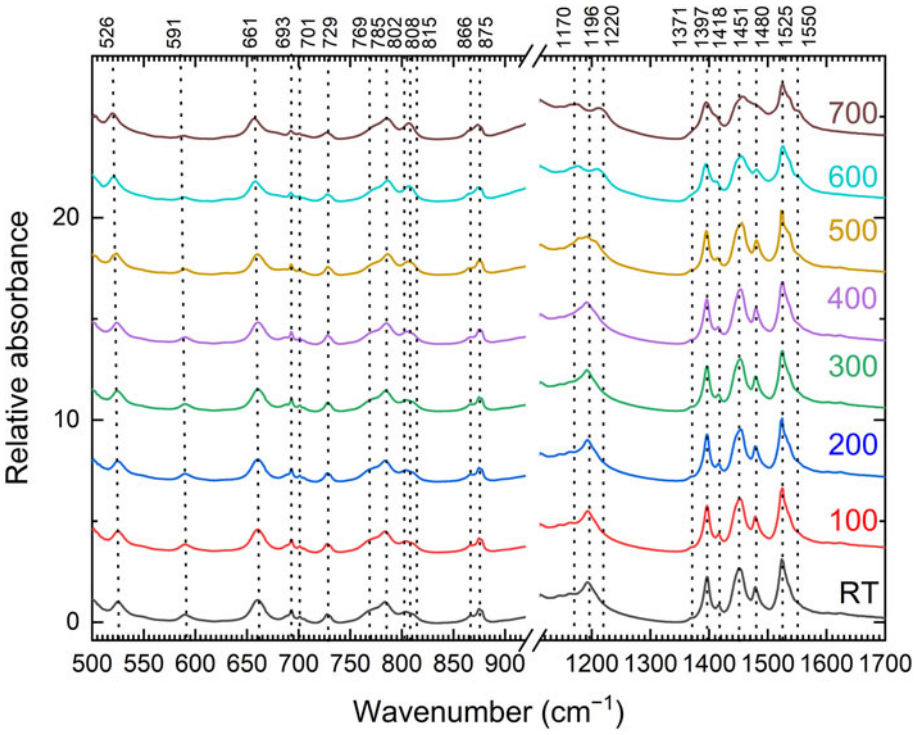

Figure 5. IR absorption spectra of fluorcarletonite annealed at different temperatures in the 500–1700 cm^{-1} range. The temperatures are given in degrees Celsius in the right side of the figure.

molecules and/or alkaline cations (e.g. McDonald and Chao 2009; Lacalamita *et al.*, 2023). In particular, in fedorite, $(K,Na)_{2.5}(Ca,Na)_7Si_{16}O_{38}(OH,F)_2{\cdot}3.5H_2O$, the tetrahedral rings of the $[Si_{16}O_{38}]^{12-}$ unit intrude the interlayer space thus hampering, during heating, the release of H_2O molecules (Lacalamita *et al.*, 2023). As a consequence, the partial dehydration of the mineral involves only a slight cell volume contraction (Lacalamita *et al.*, 2023). The crystal structure of fluorcarletonite may be related to that of fedorite as in both silicates two tetrahedral single layers are linked by an apical oxygen atom (see figure 2 in Lacalamita *et al.*, 2023 and Fig. 1, this study). However, fluorcarletonite does not contain zeolitic water. The mineral has two independent crystallographic sites occupied by the oxygens atoms of H_2O molecules coordinating Na-centred octahedra and showing very different local environments (Fig. S4). In detail, the oxygen at the O11w site is located in a cavity defined by two overlapped eight-member rings whereas the

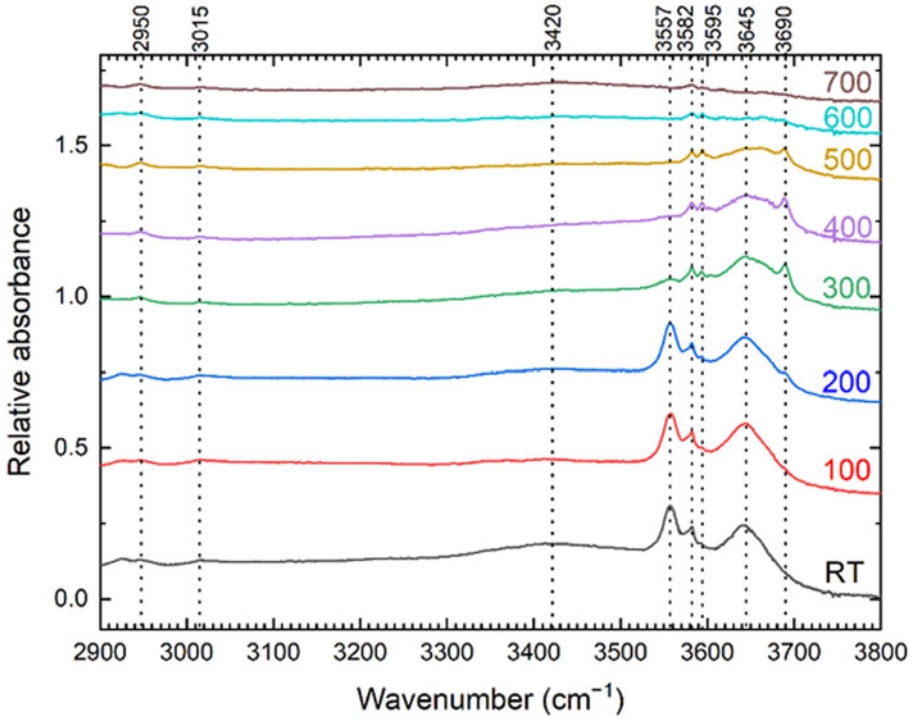

Figure 6. IR absorption spectra of fluorcarletonite annealed at different temperatures in the OH stretching vibration region. The temperatures are given in degrees Celsius in the right side of the figure.

https://doi.org/10.1180/mgm.2024.50 Published online by Cambridge University Press

Table 4. Comparison between calculated and experimental values of infrared absorption bands of fluorcarletonite at room temperature and after heating at 700°C. The band assignment is given basing on *ab initio* calculation.

Infrared band (cm^{-1})			Assignment
Experimental			
25°C	700°C	Calculated	
526	523	528	O–Si–O bending + O12w–H libration
591	587	602	O11w–H libration + O–Si–O bending
661	655	671	O–Si–O bending + O12w–H libration
693	693	698	CO_3(*C*1, *C*2) bending + O11w–H libration
701	701	701	$C1O_3$ bending
729	729	727	O–Si–O bending + O11w–H libration
769	769	765	O–Si–O bending
785	787	770	O–Si–O bending
802		789	O11w–H + O12w–H libration
808	808	794	O–Si–O bending
815			O12w–H libration
866	866	822–831	$C1O_3$ + $C2O_3$ bending (out-of-plane)
875	875		
1047	1047	1007, 1039, 1056	Si–O stretching
1147	1147	1129	Si–O stretching
1170	1170	1139	Si–O stretching
1196	1196	1168	Si–O stretching
1120	1120	1180	Si–O stretching
1397	1397	1397	$C2O_3$ stretching
1418	1418	1411	$C2O_3$ stretching
1451	1451	1458, 1460	$C1O_3$ stretching
1480	1480	1474	$C1O_3$ stretching
1525	1525	1523, 1524	$C1O_3$+$C2O_3$ stretching
1550	1550	1568–1606	O11w–H + Ow12–H bending
1600	1600		
3420	3420	3419	O11w–H stretching
3557	–	3517	O11w–H stretching
3582	3582	3571	O12w–H stretching
–	3595	3584	O6–H stretching
3645	3645	3632	O12w–H stretching
–	3690	3700	O–H stretching

oxygen at the O12w site is shared by two octahedra and statistically distributed on two symmetrically equivalent sites (O12w and O12w'), as stated above. The oxygen at the O11w site points towards the double tetrahedral layers and is bonded only to the cation at *Na*1 (Table S2). This explains its capability to shift along the *c* axis by moving away from the Na atom and to leave the crystal structure under heating conditions. Almost one half of the water content at the O11w site was, indeed, observed at 550°C with respect to that found at RT (Fig. 4; Table S1).

The oxygen at the O12w site moves toward the equivalent position at O12w' (Table 3) and, as a consequence, it approaches the two symmetrically equivalent *Na*2'-octahedra (Fig. 2). The bonding of the oxygen at the O12w site may be also affected by the cations at the *Na*2' sites. Despite a reduction of the BVS at the O12w site that was observed from 25 to 550°C (Table S2), negligible changes in BVS actually affect the O12w site if the contribution of the *Na*2' ion bond strengths is considered. This hypothesis is also in keeping with the slight decrease of the occupancy observed at the O12w site (Fig. 4; Table S1).

Therefore, fluorcarletonite upon heating to 550°C undergoes dehydration which is accompanied by a substantially isotropic enlargement of the unit cell parameters ($\Delta a = 0.53\%$ and $\Delta c = 0.55\%$) and expansion of the unit cell volume ($\Delta V = 1.6\%$). Its behaviour resembles that of framework silicates, specifically, of zeolites where the dehydration is not accompanied by significant changes in the framework structure and unit cell volume (Arletti *et al.*, 2018).

Vibrational features upon heating

The assignment of the infrared bands in Figs 5 and 6 was performed using *ab initio* calculations (Table 4).

Focusing on the tetrahedral framework, the prominent band at 1050 cm^{-1} (not shown in Fig. 5) and the less intense one at 1196 cm^{-1} are associated with Si–O stretching vibrations. The splitting of the latter band is ascribed to the thermal expansion of the tetrahedral framework during annealing. The SiO_4 bending vibrations are affected by H_2O libration modes. In detail, the shifts detected for the 526, 591 and 661 cm^{-1} bands correlate well with temperature changes and are due to the dehydration (Fig. S2). The same reason explains the variation in shape of the band in the 802–815 cm^{-1} range, probably due to the change in the position of the O11w and O12w atoms during heating.

Regarding the $(CO_3)^{2-}$ anions, the less intense band at 875 cm^{-1} may be associated with the out-of-plane bending of $(CO_3)^{2-}$. The two non-equivalent groups of $(CO_3)^{2-}$ anions have a distorted *D*3*h* point group. Therefore, at least five bands (1371–1527 cm^{-1}, Fig. 5) correspond to asymmetric stretching modes of the $(CO_3)^{2-}$ anions. In detail, *ab initio* calculations indicate that the bands at 1397 and 1480 cm^{-1} are attributed to asymmetric stretching modes of $(C2O_3)^{2-}$, whereas the bands at 1418 and 1451 cm^{-1} are related to $(C1O_3)^{2-}$. At 1525 cm^{-1} the separate closed asymmetric vibrational modes of $(C1O_3)^{2-}$ and $(C2O_3)^{2-}$ anions are not well resolved. However, the change in the angle between $(C1O_3)^{2-}$ and the *b*–*c* plane leads to a decrease in the oscillator strength of this band. This rotation and subsequent disorder of $(C1O_3)^{2-}$ anions could also explain the widening of $(C1O_3)^{2-}$ related bands. In addition, the $(C2O_3)^{2-}$ disorder associated with the shoulder at 1371 cm^{-1} results from the dehydration process. In contrast, the *C* atoms trajectories (Figs S5 and S6) obtained from the molecular dynamic simulation suggest the usual direction of vibration of C atoms, typically perpendicular to the CO_3 plane, for both *C*1 and *C*2 atoms.

Finally, the stretching vibration of the OH groups replacing fluorine provide the band at 3690 cm^{-1} that becomes detectable at $T = 200$°C and disappears at $T > 500$°C (Fig. 6; Fig. S3, curve 4) whereas the Si–O–H silanol groups give rise to the bands at 2950 and 3015 cm^{-1} that are unaffected by heating.

The adsorbed surface H_2O molecules are lost at low annealing temperatures (see the evolution of the band at 3420 cm^{-1}, in Fig. 6) whereas the structural H_2O molecules (associated with O11w and O12w) are responsible for the band at 591 cm^{-1} (libration mode) and for the shoulder at 1550 cm^{-1} (bending mode), see Fig. 5. The trajectories of the H atoms during annealing (see the deposited netCDF files) corroborate the occurrence of strong libration of the O11w and O12w.

The O11w–H groups (stretching vibration at 3557 cm^{-1}, Fig. 5) undergoes deprotonation at $T > 200$°C (Fig. S3, curve 1). The released protons interact with other oxygen atoms, mainly O6, forming new O–H bonds in which the vibrations entail the appearance of the band at 3595 cm^{-1} at $T = 200$°C that remains stable up to 500°C (Fig. S3, curve 3). The temperature behaviour of the 3595 cm^{-1} band (Fig. S3, curve 3) is similar to that of the band at 3690 cm^{-1} (Fig. S3, curve 4).

The O12w–H (stretching vibration at 3645 cm^{-1}) bonds deprotonate at $T > 600$°C (Fig. S3, curve 2).

The molecular dynamics results confirm the partial dehydration of the structure as indicated by the H atoms trajectories (Fig. S7), as well as by the Pair Distribution Function g(*r*) of the H atoms (Fig. S8). Indeed, the g(*r*) pattern at 27°C actually

https://doi.org/10.1180/mgm.2024.50 Published online by Cambridge University Press

differs from that at 327 or 627°C when the dehydration is taking place. The first peak for the $T = 27$°C case, centred around ≈1.2 Å, corresponds to the nearest neighbour shell for the O–H pair. This isolated peak (the probability g(r) drops to zero in the r range of ≈1.3–1.6 Å) for the $T = 27$ °C simulation is centred around the preferential distance between O and H atoms, that actually bind covalently, with small-amplitude vibrations around the equilibrium positions and with diffusive movements confined over small local regions, as suggested by the small spread of the peak. At higher temperatures, this Pair Distribution Function feature fails, and g(r) in the $1.3 < r < 1.6$ Å range is significantly different from zero, suggesting that random collisions between particles and great positional disorder take place. This fact is also compatible with the trends shown by the values of the mean squared displacement (msd) of the H atoms vs. time at 27, 327 and 627°C as depicted in Fig. S7: here, the high-temperature patterns are those typically determined by significant self-diffusivity, whereas the $T = 27$°C case clearly shows no diffusion at all for the H atoms.

The molecular dynamics also suggest that at 327°C some of the released H atoms (coming from the O11w–H couples) form new bonds with oxygen atoms, mainly the O6 atoms, thus producing a kind of 'isomerism', i.e. rapidly interconverting isomers. The dehydrated O11w can re-interact with an H to form a new temporary OH bond. Two snapshots of the structures at 27 and 327°C during the molecular dynamics runs after 1.8 ps and 1 ps respectively are shown in Figs S9 and S10, respectively, whereas Table S3 can be used for better understanding of the bond setup evolution with increasing temperature from 27 to 327°C.

Conclusions

At elevated temperatures, the crystal structure of fluorcarletonite undergoes dehydration and structural modifications, knowledge of which may contribute to comprehending the stability of the mineral.

Under the adopted experimental conditions, the crystal structure of fluorcarletonite is stable from RT up to ~ 150–200°C when the mineral starts to progressively dehydrate until ~550°C. The present study allows us to elucidate the mechanism of dehydration that takes place in two stages since it firstly involves the oxygen at the O11w site (at $\sim 150 \leq T \leq 550$°C) and, successively, involves the oxygen at the O12w site (mainly at $T > 500$°C). In addition, *ab initio* calculations highlight a surprising behaviour of the protons which may depart from the O11w–H groups linking with nearest oxygen atoms thus leading to perturbations of the Si–O bonds in the double tetrahedral layer.

At a temperature above 500°C the OH groups substituting the F atoms leave the crystal structure. Release of CO_2 at $T > 630$°C and defluorination at $T > 1136$°C (TG–DSC data by Kaneva *et al.*, 2020a) lead to the structure breakdown of fluorcarletonite as testified by the amorphisation of the single crystal during the *in situ* HTXRD experiment. Chao (1972) also observed amorphisation of carletonite quenched from 708°C by associating the collapse of the crystal structure to the loss of H_2O and CO_2. Defluorination of carletonite was reported to occur at much lower temperatures (300°C, see Chao, 1972) with respect to that found for fluorcarletonite (Kaneva *et al.*, 2020a).

The diffraction pattern of carletonite quenched from 775°C revealed the characteristic peaks of wollastonite ($CaSiO_3$), albite ($NaAlSi_3O_8$), $Na_2Ca_2Si_3O_9$ and $Na_2CaSi_3O_8$ (Chao, 1972). Wollastonite was also recognised as an alteration product of primary minerals in the fluorcarletonite-hosted rock under supergene conditions (Kaneva *et al.*, 2022).

The data of the present study can be integrated into a more general framework of investigations into the response to heating of a set of silicates with complex bond topology. The latter include, for instance, double-layer sheet silicates, i.e. the one based on 6^3 and 4.8^2 net, according to the silicate minerals hierarchy of Hawthorne *et al.* (2019). Indeed, fedorite (6^3 net, Hawthorne *et al.*, 2019) was recently examined (Lacalamita *et al.*, 2023) and found to exhibit a thermal behaviour very similar to that of fluorcarletonite (4.8^2 net, Hawthorne *et al.*, 2019). Therefore, it is reasonable to expect that the tetrahedral framework topology also prevents the total H_2O migration in other hydrated phases e.g. lalondeite $(Na,Ca)_6(Ca,Na)_3[Si_{16}O_{38}]F_2(H_2O)$, macdonaldite $BaCa_4[Si_{16}O_{36}(OH)_2](H_2O)_{10}$, monteregianite-(Y) $KNa_2Y[Si_8O_{19}](H_2O)_5$ and seidite-(Ce) $Na_4Ce_2Ti[Si_8O_{22}](OH)(H_2O)_5$ members of the group.

Further implications of our study concern technological applications. Indeed, changes in the crystal structure of fluorcarletonite under high temperature can lead to alterations in the absorption spectra, as well as other optical characteristics. These modifications are of utmost importance for the development of advanced optical materials, including light-emitting diodes, lasers and optical sensors, with tailored properties.

Acknowledgements. This work was supported by a M. Lacalamita grant (SIMP 2020 Research Grant in Crystal-chemistry, in memory of Prof. Fiorenzo Mazzi). The Structures Editor Peter Leverett and two anonymous referees are gratefully acknowledged for their insightful suggestions.

Supplementary material. Figures S1–S10, Tables S1–S3 and Crystallography Information Files have been deposited with the Principal Editors of *Mineralogical Magazine* and can be found at https://doi.org/10.1180/mgm.2024.50.

Competing interests. The authors declare none.

References

Arletti R., Fantini R., Giacobbe C., Gieré R., Vezzalini G., Vigliaturo R. and Quartieri S. (2018) High-temperature behavior of natural ferrierite: In-situ synchrotron X-ray powder diffraction study. *American Mineralogist*, **103**, 1741–1748.

Betteridge P.W., Carruthers J.R., Cooper R.I., Prout K. and Watkin D.J. (2003) Crystals version 12: software for guided crystal structure analysis. *Journal of Applied Crystallography*, **36**, 1487.

Bogdanov A., Kaneva E. and Shendrik R. (2021) New insights into the crystal chemistry of elpidite, $Na_2Zr[Si_6O_{15}]\cdot 3H_2O$ and $(Na_{1+y}Ca_x\square_{1-x-y})_{\Sigma=2}Zr[Si_6O_{15}]\cdot(3\text{-}x)H_2O$, and ab initio modeling of IR spectra. *Materials*, **14**, 2160.

Borovikov A.A., Vladykin N.V., Tretiakova I.G. and Dokuchits E.Yu (2018) Physicochemical conditions of formation of hydrothermal titanium mineralization on the Murunskiy alkaline massif, western Aldan (Russia). *Ore Geology Reviews*, **95**, 1066–1075.

Bray H.J., Redfern S.A.T. and Clark S.M. (1998) The kinetics of dehydration in Ca-montmorillonite: an in situ X-ray diffraction study. *Mineralogical Magazine*, **62**, 647–656.

Brese N.E. and O'Keeffe M. (1991) Bond-valence parameters for solids. *Acta Crystallographica*, **B47**, 192–197.

Brown I.D. and Altermatt D. (1985) Bond-valence parameters obtained from a systematic analysis of the Inorganic Crystal Structure Database. *Acta Crystallographica*, **B41**, 244–247.

Bruker (2007) *SAINT*. Bruker AXS Inc., Madison, Wisconsin, USA.

Bruker (2009) *SADABS*. Bruker AXS Inc., Madison, Wisconsin, USA.

Bruker (2010) *APEX2 v.2010.7-0*. Bruker AXS Inc., Madison, Wisconsin, U.S.A.

Chao G.Y. (1971) Carletonite, $KNa_4Ca_4Si_8O_{18}(CO_3)_4(F,OH)\cdot H_2O$, a new mineral from Mount St. Hilaire, Quebec. *American Mineralogist*, **56**, 1855–1866.

Chao G.Y. (1972) The crystal structure of carletonite, $KNa_4Ca_4Si_8O_8(CO_3)_4(F,OH)\cdot H_2O$, a double-sheet silicate. *American Mineralogist*, **57**, 765–778.

Gonze X., Jollet F., Abreu Araujo F., Adams D., Amadon B., Applencourt T., Audouze C., Beuken J.-M., Bieder J., Bokhanchuk A., Bousquet E., Bruneval F., Caliste D., Côté M., Dahm F., Da Pieve F., Delaveau M., Di Gennaro M., Dorado B., Espejo C., Geneste G., Genovese L., Gerossier A., Giantomassi M., Gillet Y., Hamann D.R., He L., Jomard G., Laflamme Janssen J., Le Roux S., Levitt A., Lherbier A., Liu F., Lukačević I., Martin A., Martins C., Oliveira M.J.T., Poncé S., Pouillon Y., Rangel T., Rignanese G.-M., Romero A.H., Rousseau B., Rubel O., Shukri A.A., Stankovski M., Torrent M., Van Setten M.J., Van Troeye B., Verstraete M.J., Waroquiers D., Wiktor J., Xu B., Zhou A. and Zwanziger J.W. (2016) Recent developments in the ABINIT software package. *Computer Physics Communications*, **205**, 106–131.

Hawthorne F.C. (1992) The role of OH and H_2O in oxide and oxysalt minerals. *Zeitschrift für Kristallographie*, **201**, 183–206.

Hawthorne F.C., Uvarova Y.A. and Sokolova E. (2019) A structure hierarchy for silicate minerals: sheet silicates. *Mineralogical Magazine*, **83**, 3–55.

Ivanov A.V., Vladykin N.V., Demonterova E.I., Gorovoy V.A. and Dokuchits E.Y. (2018) $^{40}Ar/^{39}Ar$ geochronology of the Malyy (Little) Murun massif, Aldan shield of the Siberian craton: A simple story for an intricate igneous complex. *Minerals*, **8**, 602.

Kaneva E. and Shendrik R. (2022) Thermal behavior of natural stellerite: high-temperature X-ray powder diffraction and IR spectroscopy study. *Analytical Sciences*, **38**, 1523–1532.

Kaneva E.V., Radomskaya T.A., Suvorova L.F. and Mitichkin M.A. (2019) Fluorcarletonite, IMA 2019-038. CNMNC Newsletter No. 51. *Mineralogical Magazine*, **83**, 757–761. doi:10.1180/mgm.2019.58.

Kaneva E., Radomskaya T., Suvorova L., Sterkhova I. and Mitichkin M. (2020a) Crystal chemistry of fluorcarletonite, a new mineral from the Murun alkaline complex (Russia). *European Journal of Mineralogy*, **32**, 137–146.

Kaneva E., Bogdanov A. and Shendrik R. (2020b) Structural and vibrational properties of agrellite. *Scientific Reports*, **10**, 15569.

Kaneva E., Radomskaya T. and Shendrik R. (2022) Fluorcarletonite – a new blue gem material. *Journal of Gemmology*, **38**, 342–351.

Kaneva E., Bogdanov A., Radomskaya T., Belozerova O. and Shendrik R. (2023) Crystal-chemical characterisation and spectroscopy of fluorcarletonite and carletonite. *Mineralogical Magazine*, **87**, 356–368.

Kasay GM. (2018) *Geology, Geochemistry and Economic Potential of the Bingo Carbonatite and its Associated Laterites in Beni, North Kivu, Democratic Republic of Congo (DRC)*. PhD dissertation, University of Nairobi, Kenya.

Kasay G.M., Bolarinwa A.T., Aromolaran O.K., Nzolang C. and Mambo V.S. (2021) A review of the geological settings, ages and economic potentials of carbonatites in the Democratic Republic of Congo. *Applied Earth Science*, **130**, 143–160.

Kresse G. and Hafner J. (1993) Ab initio molecular dynamics for liquid metals. *Physical Review B*, **47**, 558–561.

Lacalamita M., Mesto E., Kaneva E., Shendrik R., Radomskaya T. and Schingaro E. (2023) High temperature behavior of fedorite, $Na_{2.5}(Ca_{4.5}Na_{2.5})[Si_{16}O_{38}]F_2\cdot 2.8H_2O$, from the Murun Alkaline Complex, Russia. *Mineralogical Magazine*, **87**, 542–553.

McDonald A. and Chao G.Y. (2009) Lalondeite, a new hydrated Na–Ca fluorosilicate species from Mont Saint-Hilaire Quebec: description and crystal structure. *The Canadian Mineralogist*, **47**, 181–191.

Perdew J.P., Ruzsinszky A., Csonka G.I., Vydrov O.A., Scuseria G.E., Constantin L.A., Zhou X. and Burke K. (2008) Restoring the density-gradient expansion for exchange in solids and surfaces. *Physical Review Letters*, **100**, 136406.

Post J.E., Bish D.L. and Heaney P.J. (2015) Synchrotron powder X-ray diffraction study of the structure and dehydration behavior of sepiolite. *American Mineralogist*, **92**, 91–97.

Shannon R.D. (1976) Revised effective ionic radii and systematic studies of interatomic distances in halides and chalcogenides. *Acta Crystallographica*, **A32**, 751–767.

Togo A. and Tanaka I. (2015) First principles phonon calculations in materials science. *Scripta Materialia*, **108**, 1–5.

Vladykin N.V. (2009) Potassium alkaline lamproite-carbonatite complexes: Petrology, genesis, and ore reserves. *Russian Geology Geophysics*, **50**, 1119–1128.

Vladykin N.V., Borokovikov A.A., Dokuchits E.Yu. and Thomas V.G. (2018) Genesis of charoite rocks in the Murun massif, Aldan Shield, Russia. *Geochemistry International*, **56**, 1135–1147.

Zema M., Ventruti G., Lacalamita M. and Scordari F. (2010) Kinetics of Fe-oxidation/deprotonation process in Fe-rich phlogopite under isothermal conditions. *American Mineralogist*, **95**, 1458–1466.

Zema M., Ventruti G., Tarantino S. and Micelli C. (2022) A new thermal and atmospheric conditioning device for in situ single-crystal diffraction is up and running. Pp. S18–21 in: *Book of Abstract of the Congress on Geosciences for a Sustainable Future*. Società Geologica Italiana e Società Italiana di Mineralogia e Petrologia, Torino, Italy.

https://doi.org/10.1180/mgm.2024.50 Published online by Cambridge University Press